

Scalable Integration of Indium Zinc Oxide/Photosensitive-Nanowire Composite Thin-Film Transistors for Transparent Multicolor Photodetectors Array

Xingqiang Liu, Lang Jiang, Xuming Zou, Xiangheng Xiao, Shishang Guo, Changzhong Jiang, Xi Liu, Zhiyong Fan, Weida Hu, Xiaoshuang Chen, Wei Lu, Wenping Hu,* and Lei Liao*

Unique transparent phototransistors can be placed on portable devices, serving as optical sensors while allowing light to pass through and transparency/visibility to be maintained. Bottom-up assembly of nanoscale materials can be utilized as building blocks for fabrication of such devices with novel function. Recently, one-dimensional nanowires (NWs) and graphene have been employed as the alternative active-detection matrix to fabricate transparent photodetectors with high sensitivity.^[1–4] However, the challenging procedures of arranging the NWs with good alignment and large-scale uniformity limit their practicality.^[5,6] On the other hand, red, green, and blue are the primary colors of light, which can be mixed in different proportions to produce a wide range of other additive colors. Thus, it is urgent to explore photodetectors that are sensitive to these three colors.^[7–10] Although graphene has a broadband photoelectric response covering the visible to infrared regions, which is tunable by modulating the Fermi level,^[11,12] it has a

low responsivity and no spectral selectivity. Meanwhile, transparent amorphous metal oxide materials have gained much attention in recent years. Tremendous effort has been focused on improving the mobility,^[13–15] threshold voltage,^[16,17] stability^[18,19] and/or mechanical flexibility^[20–22] for implementation of transparent thin-film transistors (TFTs). They can not only potentially replace silicon in many conventional applications, but also enable emerging glass/paper electronics.^[3,4,23] Due to their wide-bandgap nature, amorphous metal oxides (e.g., amorphous indium zinc oxide (a-IZO)) are typically insensitive to visible light, having weak optical absorption.^[24,25] Thus they need to be tailored to enhance absorption in the visible region for transparent multicolor photodetectors.

In this work, photosensitive CdS, CdSeS, and CdSe NWs were incorporated into the a-IZO thin films. It was found that these crystalline NWs not only improved the mobility of a-IZO TFTs, but also rendered them responsive to visible light. Furthermore, we have demonstrated that an a-IZO/CdS NWs TFT array can serve as a transparent image sensor. The composite devices have leveraged the advantages of the transparency of the a-IZO with the photosensitivity of the NWs, and our fabrication scheme can effectively avoid challenging procedures to arrange the NWs with good alignment. Along with high reproducibility and scalability, this type of metal oxide/photosensitive NW TFT offers a unique route toward miniaturization of photodetectors while maintaining their functionality, and presents a potential paradigm shift in large-scale transparent image sensors. Through engineering the bandgap of the incorporated photosensitive NWs, multicolor photodetectors can be effectively designed and fabricated.

Figure 1 shows a schematic of the fabrication of the a-IZO/NWs composite TFTs. Crystalline photosensitive NWs were prepared following a typical chemical vapor deposition method^[24] and examined by X-ray diffraction (Supporting Information, Figure S1a–c). The as-prepared NWs with specified weight concentrations (from 0 to 0.9% varied systematically) were dispersed into the precursors, and the composite thin films were fabricated via a sol-gel approach. Finally, source/drain electrodes were fabricated by standard photolithography, followed by metallization and lift-off processes.

It is known that an image sensor should consist of an array of photodetectors that are sensitive to light with at least three primary colors. Herein, evident absorption for these colors was demonstrated with the photosensitive NWs (**Figure 2a**) which were later employed to improve the photoresponse of the a-IZO

Dr. X. Q. Liu, Dr. X. M. Zou, Prof. X. H. Xiao,
Prof. S. S. Guo, Prof. C. Z. Jiang, Prof. L. Liao
Department of Physics and Key Laboratory
of Artificial Micro- and Nano-structures
of Ministry of Education
Wuhan University
Wuhan 430072, China
E-mail: liaolei@whu.edu.cn

Dr. L. Jiang, Prof. W. P. Hu
Beijing National Laboratory for Molecular Sciences
Key Laboratory of Organic Solids
Institute of Chemistry
Chinese Academy of Sciences
Beijing 100080, China
E-mail: huwp@iccas.ac.cn

Dr. X. Liu, Prof. Z. Y. Fan
Department of Electronic & Computer Engineering
The Hong Kong University of Science & Technology
Hong Kong SAR, China

Prof. W. D. Hu, Prof. X. S. Chen, Prof. W. Lu
National Laboratory for Infrared Physics
Shanghai Institute of Technical Physics
Chinese Academy of Sciences
Shanghai 200083, China

Prof. W. D. Hu, Prof. X. S. Chen, Prof. W. Lu
Synergetic Innovation Center of Quantum
Information & Quantum Physics
University of Science and Technology of China
Hefei, Anhui 230026, China



DOI: 10.1002/adma.201305073

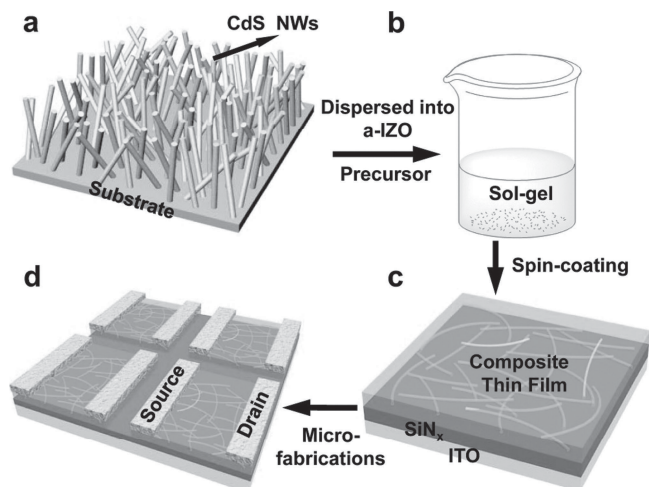


Figure 1. Schematic illustration of the fabrication process to obtain a-IZO/CdS NWs composite thin film transistors. a) The CdS NWs synthesized on SiO₂/Si substrate. b) The CdS NWs were introduced into the a-IZO precursor and ultrasonically dispersed so as to achieve a uniform composite precursor. c) The a-IZO/CdS NWs composite thin films were obtained by a spin-coating method. d) Typical a-IZO/CdS NWs composite device array.

thin films. The corresponding photoluminescence spectra are shown in Figure S1d. Figure 2b–d shows scanning electron microscopy (SEM) images of the as-prepared CdS, CdSeS, and CdSe NWs respectively. These images reveal the formation of one-dimensional NWs tens of micrometers in length and

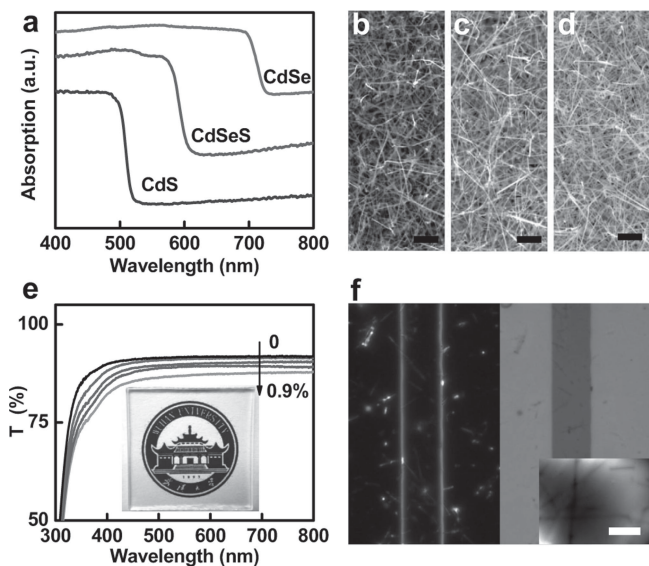


Figure 2. Characterization of the photosensitive NWs used in this work. a) UV-vis diffuse reflectance spectra of the as-prepared CdS, CdSeS, and CdSe NWs used in this work. b–d) SEM images of the CdS (b), CdSeS (c), and CdSe NWs (d); the scale bars are all 2 μm. e) The UV-vis transmittance spectra of the composite thin film with the weight percentage of CdS NWs systematically varied from 0 to 0.9 wt%; the inset image is an optical image of the transparent a-IZO/CdS NWs composite thin film on ITO glass. f) The optical bright/dark field images of the a-IZO/CdS NWs composite TFT, the channel length is 5 μm. The inset is a typical TEM image of the a-IZO/CdS NWs composite thin film; the scale bar is 100 nm.

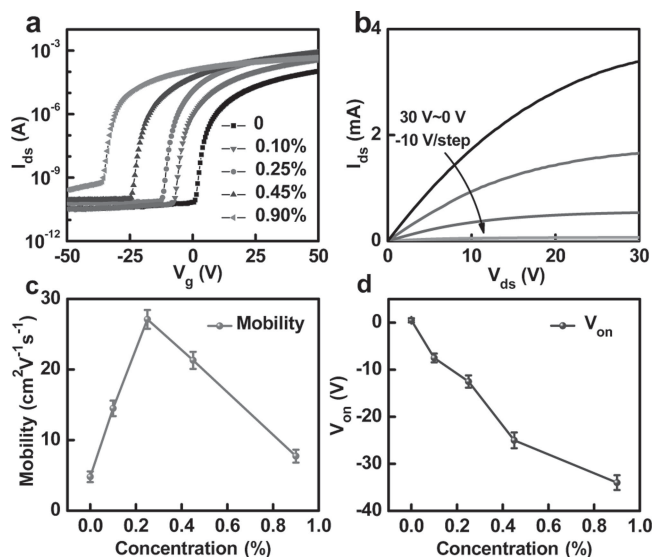


Figure 3. Typical electrical characteristics of a-IZO/CdS NW composite TFTs with different CdS NW weight concentrations. a) Transfer characteristics (with I_{ds} plotted logarithmically) at $V_{ds} = 2$ V. b) Typical output characteristics of the a-IZO/CdS composite TFTs with 0.25% CdS NWs. c) Plot of mobility vs. CdS NW concentration. d) Plot of V_{on} vs. CdS NW concentration; the error bars in (c) and (d) indicate the standard deviation over 15 devices.

40–60 nm in diameter. As a comparison, a single CdS nanowire transistor is shown in Figure S2 in the Supporting Information. Figure 2e shows the representative UV-vis transmittance spectra of the composite thin films with different weight percentages of CdS NWs, varying from 0 to 0.9%. The fabricated composite thin films exhibit desired transparency in the visible region, showing their potential for fabricating transparent electronics (inset of Figure 2e). Figure 2f shows the dark-field and bright-field optical images (integral time were fixed to be 2 s) of the device with 0.9 wt% CdS NWs. The transmission electron microscopy (TEM) image in the inset shows the CdS NWs embedded in the composite thin film.

To evaluate the effects of the incorporated crystalline photosensitive NWs in the a-IZO/CdS NW composite thin films, electrical measurements were carried out under dark conditions. Typical transfer curves of the a-IZO/CdS NW TFTs with different CdS NW concentrations are shown in Figure 3a, indicating that the ON current is significantly enhanced following the incorporation of the CdS NWs. The increased number of traps located in the composite thin films and the interface with the bulk dielectric layer may result in an increment of the hysteresis and subthreshold slope (Figure S3b, Supporting Information).^[26,27] Figure 3b shows the corresponding output characteristics of the fabricated a-IZO/CdS NW TFTs with 0.25 wt% CdS NWs. The saturation and conspicuous pinch-off characteristics indicate that the active channel can be largely modulated by the gate bias. Specifically, the composite TFTs possess controllable dark-state electrical characteristics. Figure 3c,d summarize the effects of the concentration of the CdS NWs on the device electrical properties. The TFTs show increased field-effect mobility with CdS NW concentration up to 0.25% and reach a peak value of 27.1 cm² V⁻¹ s⁻¹. Beyond 0.25%, the mobility decreases with increasing CdS NW concentration.

This observation can be explained by the following rationale: in the ON state, the crystalline CdS NWs shorten the channel length and/or provide fast carrier-transport tracks at low concentration. On the other hand, having more incorporated CdS NWs in the a-IZO films apparently induces more defects at the oxide/NW interface. This may lead to more carrier traps and boundaries, giving rise to increased contact resistance between the CdS NWs and the a-IZO. Thus, injection of carriers is inhibited and the turn-on voltage (V_{on}) drifts to more-negative values, resulting in inferior TFT performance.^[28–31] Meanwhile, the a-IZO/CdSeS NW TFTs and a-IZO/CdSe NW TFTs demonstrated similar performance to those of the a-IZO/CdS NW TFTs (Figure S4, Supporting Information). Moreover, the a-IZO/NWs composite TFTs have shown excellent stability over time in atmospheric conditions, with the devices maintaining stable transfer characteristics after 21 days, as shown in Figure S5 in the Supporting Information.

It is known that CdS NWs, with a 2.4 eV bandgap, are sensitive to blue-light illumination, demonstrated by the photosensitivity of the CdS NW TFTs under 445 nm laser illumination (Figure S6, Supporting Information). To confirm the critical role of the photosensitive NWs for achieving improved photoelectrical properties, the electrical transport properties of the a-IZO/CdS NW TFTs with 0.25% NWs under 445 nm wavelength illumination are shown in Figure S7a in the Supporting Information. The V_{on} of the device drifted to a more-negative value when the light was switched on. Meanwhile, when the a-IZO/CdS NW TFT was illuminated under a 445 nm-wavelength laser source (Figure 4a), a specific $V_g = -15$ V was required to deplete the channel carriers to maximize the photocurrent gain (Figure S7b), allowing the photogenerated carriers to drift through the channel. In this scheme, the photoresponse

ratio (I_{light}/I_{dark}) is much more sensitive to carrier-concentration change caused by light illumination.^[30] Finally, the signal can be read by applying a 0.1 V source–drain voltage (Figure S7c). Due to the weak absorption of the laser light, the pristine a-IZO TFT presented a photocurrent of 0.5 nA after a long illumination period (Figure S8, Supporting Information), showing poor photoresponse. The a-IZO/CdS NW composite TFTs exhibited an evident photocurrent with a quick response time (Figure 4b). Additionally, the oxide semiconductor has a critical drawback associated with oxygen vacancies (i.e., defects), which enhance the channel conductivity by liberating electrons, causing the persistent asymmetric photocurrent.^[32–34] Moreover, Figure S9a in the Supporting Information presents evidence of the photocurrent versus illumination wavelength in the range of ca. 400–800 nm. Figure S9b shows the increase in photocurrent of the a-IZO/CdS NW TFTs with illumination intensity. In other words, the incorporated photosensitive CdS NWs rendered the a-IZO films with a superior photoresponse property. The a-IZO/CdSeS and a-IZO/CdSe NW composite TFTs were also found to be sensitive to 532 nm and 650 nm laser illumination, respectively, as shown in Figure 4c,d. The photocurrent measurements indicate the feasibility of enhancing the photoresponsivity by mixing photosensitive NWs with an a-IZO thin film. This phenomenon can be understood on the basis of the following rationale. There are two processes occurring when an a-IZO/CdS NW TFT is illuminated with photons having an energy higher than the bandgap of CdS (Figure S8d). The laser-illumination-induced photogenerated electron–hole pairs in the CdS NWs and a-IZO provided continuous conduction pathways for carrier transport. Moreover, CdS and a-IZO are in good energy-band alignment. The conduction-band edges of ZnO and In_2O_3 are located between the conduction

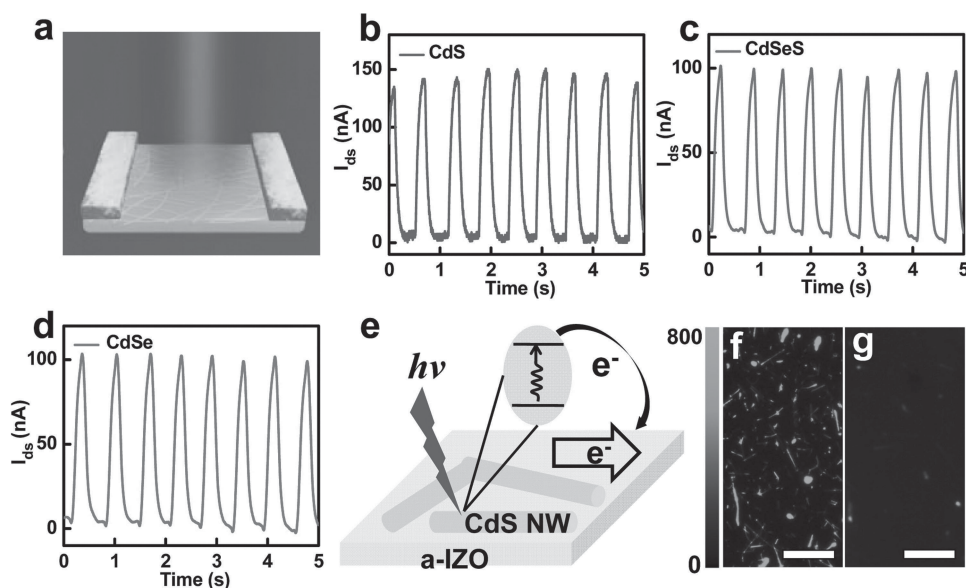


Figure 4. Photoresponse of the multicolor photodetector. a) The schematic diagram of the photoresponse test. b–d) The on–off photoresponse of a-IZO/CdS, a-IZO/CdSeS, and a-IZO/CdSe NW composite TFTs with 0.25 wt% NWs. The illumination intensities are fixed to be 25 mW mm^{-2} for all the measurements. e) Schematic illustration of light-induced charge excitation in photosensitive CdS NWs, followed by charge transport along the a-IZO thin film. f,g) Fluorescence images of CdS NWs and the a-IZO/CdS composite thin films, respectively, on glass substrate. The grayscale scale bar indicates the number of emitted photons (in arbitrary units) integrated over 100 ms (488 nm as the excitation wavelength in all the fluorescence experiments); the scale bar is 10 μm .

band and the valence band of the CdS. In this band configuration, upon illumination with sufficient incident photon energy ($h\nu > E_g$), electrons can be excited to the conduction band of the CdS NWs, and the photogenerated electrons in the CdS NWs can be easily transferred to the conduction band of the a-IZO thin film (Figure S8d). The applied source–drain voltage separates the electrons and holes to the opposite terminals. In this scenario, charge separation is achieved and the free carrier concentration is increased. Thus it is much more difficult to pinch off the active a-IZO/CdS NW channel, and hence the V_{on} shifts to a more-negative value. By using such a composite thin film as the channel layer, photogenerated carriers can be efficiently transferred from photosensitive NWs, such as CdS, CdSeS, and CdSe (donor), to a-IZO (acceptor) leading to the increased photogenerated current (Figure 4e). The a-IZO/photosensitive NW hybrid system showed reasonable photoresponse to illumination with white light and light having a wavelength of 532 nm (Figure S10, Supporting Information), which demonstrated the feasibility for multicolor image sensing. The charge transfer also results in photoluminescence quenching of the NWs in composite thin films. Images of the individual CdS NWs on a glass substrate and the a-IZO/CdS NW composite thin film with a color scale-bar indicating the fluorescence intensity are shown in Figure 4f,g respectively. The CdS NWs show strong fluorescence; however, the composite thin film reveals fluorescent quenching.

In order to verify the scalability of the fabrication scheme, a large-scale transparent image sensor containing an a-IZO/CdS NW composite TFT array (18 pixels \times 22 pixels) was fabricated on 200 nm SiN_x-coated indium tin oxide (ITO) glass (Figure 5a). One of the most important figures-of-merit for a photodetector is the photoresponsivity. Figure 5b shows the photoresponse curve acquired at a bias voltage of $V_{ds} = 0.1$ V, and a back-gate voltage of $V_g = -15$ V (Figure 5b).

At high illumination intensities (25 mW mm⁻²), the device reaches a photoresponsivity of 54.2 mA W⁻¹ (Figure 5c), which is comparable to that of amorphous-silicon-based photodetectors^[35] and 108 times higher than that of the first graphene photodetectors.^[36] To determine the sensitivity of the photodetectors under illumination pulses, we have measured the transient response of the a-IZO/CdS NW TFTs with different CdS NW concentrations. Figure 5d shows the overall photocurrent of the devices obtained under global laser illumination with a frequency of 100 Hz. Since high mobility leads to fast carrier transportation, the photocurrent follows the mobility trend very well (Figure 5e). As a proof of concept to demonstrate that a-IZO/NW composite thin-film devices can readily function as image sensors, light fringes (Supporting Information, Figure S11a) were projected onto the center of the TFT array (Figure 5a). The output current was measured for each individual TFT. Approximately 99.2% of the TFTs in the array were functional, while only three devices failed to work. In this case, each of the TFTs can serve as a pixel, and the measured conductance of the TFTs was incorporated into a 2D plot to generate a contrast map, as shown in Figure 5f. The contrast map clearly demonstrates the spatial intensity distribution from the bright fringes to the dark fringes, thus showing its preliminary imaging function. Meanwhile, a Gauss light (Supporting Information, Figure S12a) was focused and projected onto the TFTs array (18 pixels \times 18 pixels), and the 2D contrast maps (Supporting Information, Figure S12b,c) precisely reflects the intensity profile of the projected light source.

In summary, we have demonstrated a simple and robust sol-gel process for combining a-IZO with photosensitive NWs (including CdS, CdSeS and CdSe NWs). Not only was the carrier mobility enhanced by the incorporated photosensitive crystalline NWs, but also the photosensitivity was improved, when compared with that of pristine a-IZO TFTs. The transparent

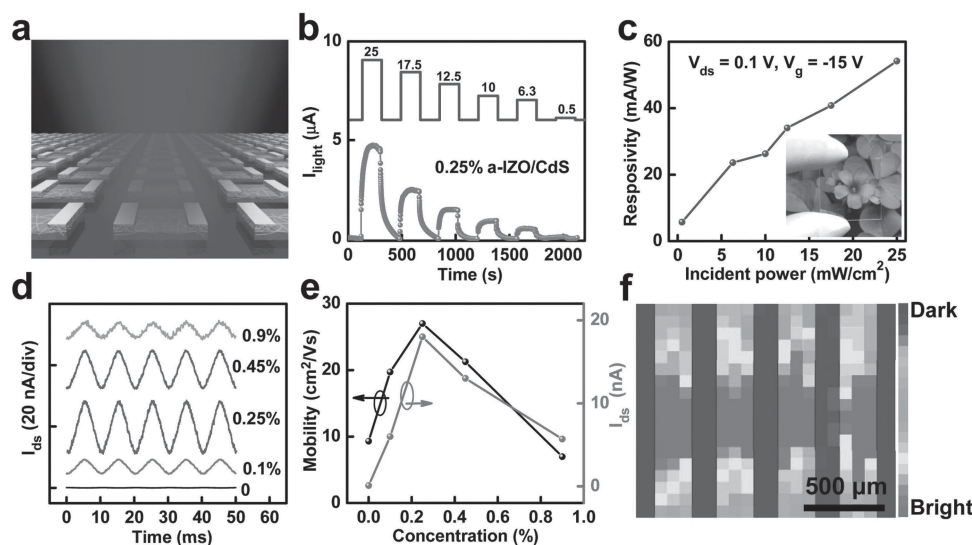


Figure 5. Typical photoresponse characteristics of the a-IZO/CdS NWs TFTs array fabricated on SiN_x/ITO glass substrate. a) Perspective picture showing the imaging function of the TFTs array. b) The long-term transient response plots of the a-IZO/CdS NW TFTs with different incident powers. The numbers in the figure indicate the incident power, in units of mW mm⁻². c) Plot of the responsivity with different incident power; the inset shows an optical image of the a-IZO/CdS NW composite TFTs fabricated on glass, showing its transparency. d) The 100 Hz transient photoresponse curve of the a-IZO/CdS NW TFTs with different CdS NWs on SiN_x/ITO transparent substrates. e) The plots of mobility and I_{on} vs. CdS NW concentration. f) An output response of the TFT array, imaging periodic light fringes. The contrast represents the normalized conductance.

TFT array shows potential for large-scale visible-light image sensing. Considering the excellent uniformity, and the facile and reproducible fabrication processes, the concept can be extended to the fabrication on glass of transparent multicolor photodetectors and optoelectronic switches.

Experimental Section

Preparation of NWs: All the NWs used in this work were synthesized using a chemical vapor deposition method based on the vapor–liquid–solid mechanism. NW growth was carried out in a single-zone horizontal tube furnace with Ar gas (99.99%) as the carrier and protection gas. SiO₂/Si coated with 1 nm of Au was used as the growth substrate for preparing CdS NWs, and CdS powder was used as the source. After 20 min of purging, the furnace was heated for 30 min at 850 °C with an Ar gas rate of 200 sccm. The furnace was then cooled to room temperature naturally. Finally, CdS NWs were obtained on the substrate with a uniform composition across the whole substrate. To grow CdSe NWs, Si substrates coated with a 0.8 nm Ni film were used as the growth substrates. A mixture of CdSe and CdS at a molar ratio of 1:1 was used as the source. The furnace was then heated at 820 °C for 30 min with the same growth conditions as those for CdS NWs. The CdSe NWs were synthesized at 780 °C for 30 min with the same conditions as those for CdSe NWs. All the NWs were of good uniformity, with a length of tens of micrometers, and a diameter of 40–60 nm.

Precursor Preparation: Metal precursors were dissolved in a solution of ethanolamine and ethanolamine/2-methoxyethanol with volume ratio of 0.92:100. The molar ratio of In:Zn was set as 1:1, whereas the total concentration of metal ions was maintained at 0.03 M. After 2 h of vigorous stirring, a stable, transparent solution was formed for each precursor solution. Finally, the as-prepared NWs with specific weight concentrations were dispersed in solutions by an ultrasonic process for 5 min.

Thin-Film Deposition: 100 nm of SiO₂/p⁺-Si wafers and ITO glass with 200 nm SiN_x layers was used as the starting substrates. The cut pieces were thoroughly washed with copious amounts of anhydrous ethanol and dried with a N₂ blower. The clean substrates were further treated with oxygen plasma for 5 min. The a-IZO/NWs thin films were formed by a spin-coating method at a speed of 3000 rpm for 60 s. Then, the films were prebaked on a hotplate at 150 °C for 10 min to remove the organic solvent. This process was repeated 3 times to achieve the desired thickness. Finally, the as-prepared thin films were annealed on a hotplate at 400 °C for 40 min under ambient conditions.

TFT Fabrication and Microscopy Characterization. Two-step photolithography was employed to fabricate the TFTs. First, photolithography and a wet etch (dipped into 10% HCl etchant for 2 min) were carried out to divide the as-prepared thin film into isolated pads that could suppress the gate leakage current. The second step of the photolithography was conducted to define the source and drain electrodes (S/D). The Cr/Au (15 nm/40 nm) electrodes were deposited using a thermal evaporator for the electrical measurements on SiO₂/Si substrates. To fabricate the transparent photodetector array, fabricated on glass, a 70 nm-thickness of ITO was deposited by magnetron sputtering, and was employed as the transparent source/drain electrodes. Electron beam lithography (JEOL 6510 with NPGS) was employed to fabricate a single NW device. The optical images were captured using an Olympus BX51M microscope. The fluorescence images were taken using an Olympus IX81 instrument. TEM images were taken using a JEOL JEM-2010 instrument.

Electrical Measurements: Electrical measurements were performed using a Lake Shore TTPX probe station and an Agilent 4155C semiconductor parameter analyzer. For the transport characteristics under dark conditions, p⁺-Si served as the back gate electrodes and the gate bias was swept from –50 V to 50 V, and then back to –50 V continuously.

For all the photoresponse tests, the channel was first depleted by a default gate bias (the mean value of the V_{on} under dark conditions

and on laser illumination) on the back-gate electrode (p⁺-Si or ITO). For long-term photoresponse measurements, a mechanical chopper in front of the laser was driven by an adjustable power supply. A specific attenuation partition was inserted into the light path to reduce the illumination power. Finally, a source–drain voltage of 0.1 V was set to read out the signal. The 100 Hz photoresponse measurements were carried out by combining an NI data acquisition board and an Agilent DSO-X2022A digital storage oscilloscope, and the measurement scheme was same as that of the long-term photoresponse measurements.

Supporting Information

Supporting Information is available from the Wiley Online Library or from the author.

Acknowledgements

The authors acknowledge the 973 grant of MOST (No. 2011CB932704 and 2013CB632705), MOE (NCET-10-0643 and 20120141110054), NSFC grant (Nos. 11104207, 61222402, 91123009, 10990103 and 11322441), Hubei Province Natural Science Foundation (2011CDB271), the Natural Science of Jiangsu Grant (BK2011348), GRF 623112 from the Hong Kong Research Grant Council, as well as Fundamental Research Funds for the Central Universities (No. 2012202020205).

Received: October 11, 2013

Revised: November 15, 2013

Published online:

- [1] Z. Fan, J. C. Ho, Z. A. Jacobson, H. Razavi, A. Javey, *Proc. Natl. Acad. Sci. USA* **2008**, *105*, 11066.
- [2] F. Zhang, Y. Ding, Y. Zhang, X. Zhang, Z. L. Wang, *ACS Nano* **2012**, *6*, 9229.
- [3] T. Dufaux, M. Burghard, K. Kern, *Nano Lett.* **2012**, *12*, 2705.
- [4] L. Dong, S. Niu, C. Pan, R. Yu, Y. Zhang, Z. L. Wang, *Adv. Mater.* **2012**, *24*, 5470.
- [5] J. Jie, W. Zhang, Y. Jiang, X. Meng, Y. Li, S. Lee, *Nano Lett.* **2006**, *6*, 1887.
- [6] E. M. Fortunato, P. M. Barquinha, A. Pimentel, A. M. Gonçalves, A. J. Marques, L. M. Pereira, R. F. Martins, *Adv. Mater.* **2005**, *17*, 590.
- [7] X. Gong, M. Tong, Y. Xia, W. Cai, J. S. Moon, Y. Cao, G. Yu, C.-L. Shieh, B. Nilsson, A. J. Heeger, *Science* **2009**, *325*, 1665.
- [8] K. Banger, Y. Yamashita, K. Mori, R. Peterson, T. Leedham, J. Rickard, H. Sirringhaus, *Nat. Mater.* **2010**, *10*, 45.
- [9] J. S. Park, W.-J. Maeng, H.-S. Kim, J.-S. Park, *Thin Solid Films* **2012**, *520*, 1679.
- [10] S. Ju, J. Li, J. Liu, P.-C. Chen, Y.-g. Ha, F. Ishikawa, H. Chang, C. Zhou, A. Facchetti, D. B. Janes, *Nano Lett.* **2007**, *8*, 997.
- [11] Z. Li, E. A. Henriksen, Z. Jiang, Z. Hao, M. C. Martin, P. Kim, H. Stormer, D. N. Basov, *Nat. Phys.* **2008**, *4*, 532.
- [12] F. Wang, Y. Zhang, C. Tian, C. Girit, A. Zettl, M. Crommie, Y. R. Shen, *Science* **2008**, *320*, 206.
- [13] H. W. Zan, C. C. Yeh, H. F. Meng, C. C. Tsai, L. H. Chen, *Adv. Mater.* **2012**, *24*, 3509.
- [14] H. Yabuta, M. Sano, K. Abe, T. Aiba, T. Den, H. Kumomi, K. Nomura, T. Kamiya, H. Hosono, *Appl. Phys. Lett.* **2006**, *89*, 112123.
- [15] D. H. Lee, Y. J. Chang, G. S. Herman, C. H. Chang, *Adv. Mater.* **2007**, *19*, 843.
- [16] J. K. Jeong, J. H. Jeong, H. W. Yang, J.-S. Park, Y.-G. Mo, H. D. Kim, *Appl. Phys. Lett.* **2007**, *91*, 113505.

- [17] Y. Kwon, Y. Li, Y. Heo, M. Jones, P. Holloway, D. Norton, Z. Park, S. Li, *Appl. Phys. Lett.* **2004**, *84*, 2685.
- [18] D.-H. Kim, D.-H. Son, S.-J. Sung, J.-H. Kim, J.-K. Kang, *Mol. Cryst. Liq. Cryst. Sci. Technol.* **2012**, *564*, 130.
- [19] J. C. Park, S. Kim, S. Kim, C. Kim, I. Song, Y. Park, U. I. Jung, D. H. Kim, J. S. Lee, *Adv. Mater.* **2010**, *22*, 5512.
- [20] X. Liu, C. Wang, B. Cai, X. Xiao, S. Guo, Z. Fan, J. Li, X. Duan, L. Liao, *Nano Lett.* **2012**, *12*, 3596.
- [21] M. J. Gadre, T. Alford, *Appl. Phys. Lett.* **2011**, *99*, 051901.
- [22] K. Chiba, A. Futagami, *Appl. Phys. Lett.* **2008**, *93*, 013114.
- [23] K. Nomura, H. Ohta, A. Takagi, T. Kamiya, M. Hirano, H. Hosono, *Nature* **2004**, *432*, 488.
- [24] K. Nomura, H. Ohta, K. Ueda, T. Kamiya, M. Hirano, H. Hosono, *Science* **2003**, *300*, 1269.
- [25] Y. Sun, J. A. Rogers, *Adv. Mater.* **2007**, *19*, 1897.
- [26] J.-M. Lee, I.-T. Cho, J.-H. Lee, H.-I. Kwon, *Appl. Phys. Lett.* **2008**, *93*, 093504.
- [27] T.-C. Chen, T.-C. Chang, T.-Y. Hsieh, W.-S. Lu, F.-Y. Jian, C.-T. Tsai, S.-Y. Huang, C.-S. Lin, *Appl. Phys. Lett.* **2011**, *99*, 022104.
- [28] W. Lim, E. Douglas, S.-H. Kim, D. Norton, S. Pearton, F. Ren, H. Shen, W. Chang, *Appl. Phys. Lett.* **2009**, *94*, 072103.
- [29] X. Duan, C. Niu, V. Sahi, J. Chen, J. W. Parce, S. Empedocles, J. L. Goldman, *Nature* **2003**, *425*, 274.
- [30] G.-W. Hsieh, F. M. Li, P. Beecher, A. Nathan, Y. Wu, B. S. Ong, W. I. Milne, *J. Appl. Phys.* **2009**, *106*, 123706.
- [31] S. Kumar, G. Blanchet, M. Hybertsen, J. Y. Murthy, M. A. Alam, *Appl. Phys. Lett.* **2006**, *89*, 143501.
- [32] S. Jeon, S.-E. Ahn, I. Song, C. J. Kim, U.-I. Chung, E. Lee, I. Yoo, A. Nathan, S. Lee, J. Robertson, *Nat. Mater.* **2012**, *11*, 301.
- [33] K. Ghaffarzadeh, A. Nathan, J. Robertson, S. Kim, S. Jeon, C. Kim, U.-I. Chung, J.-H. Lee, *Appl. Phys. Lett.* **2010**, *97*, 143510.
- [34] M. Liao, Y. Koide, J. Alvarez, M. Imura, J.-P. Kleider, *Phys. Rev. B* **2008**, *78*, 045112.
- [35] D. Caputo, G. de Cesare, A. Nascetti, R. Negri, R. Scipinotti, *IEEE Sensors J.* **2007**, *7*, 1274.
- [36] F. Xia, T. Mueller, Y.-m. Lin, A. Valdes-Garcia, P. Avouris, *Nat. Nanotechnol.* **2009**, *4*, 839.